Biophysical Journal, Volume 99

Supporting Material

Title: How to Squeeze a Sponge: Casein Micelles under Osmotic Stress, a SAXS Study

Authors: Antoine Bouchoux, Geneviève Gésan-Guiziou, Javier Pérez, and Bernard Cabane

Supporting Material

How to Squeeze a Sponge: Casein Micelles under Osmotic Stress, a SAXS Study

Antoine Bouchoux,[†‡*] Geneviève Gésan-Guiziou,[†‡] Javier Pérez,[§] and Bernard Cabane[¶*]

[†]INRA, UMR1253 Science et Technologie du Lait et de l'Œuf, F-35042 Rennes, France; [‡]Agrocampus Ouest, UMR1253 Science et Technologie du Lait et de l'Œuf, F-35042 Rennes, France; [§]Synchrotron SOLEIL, Orme Merisiers, F-91192 Gif Sur Yvette, France; and [¶]PMMH, CNRS UMR7636, ESPCI, F-75231 Paris cedex 05, France

[*]Correspondence: antoine.bouchoux@rennes.inra.fr and bcabane@pmmh.espci.fr

Note S1: Quantitative evaluation of structural models

S1-1 *Homogeneous* model

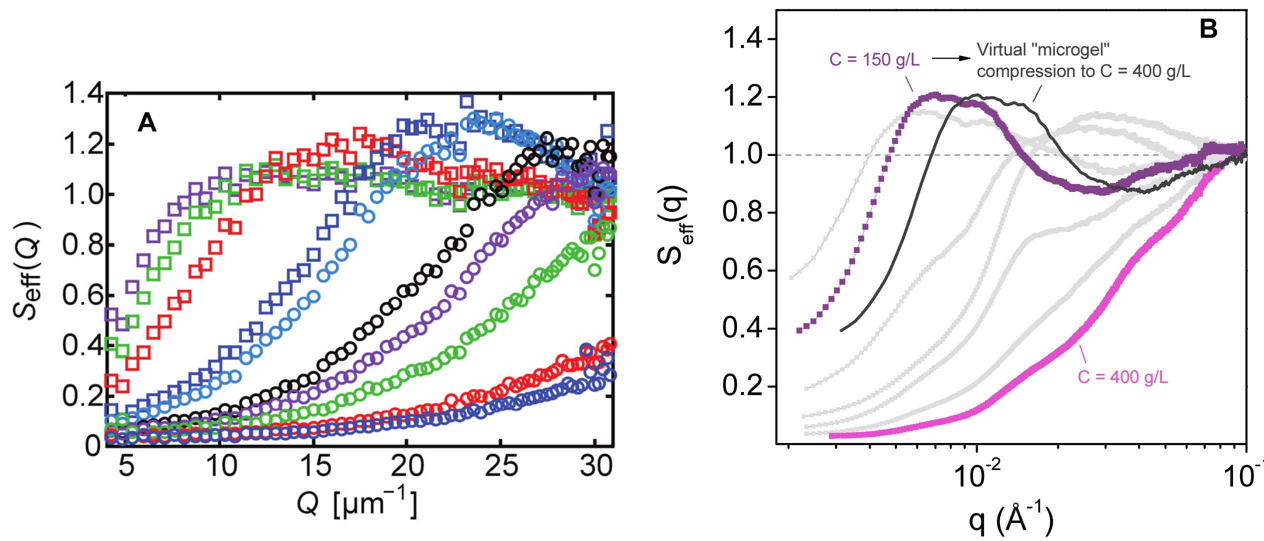

FIGURE S1 (*A*) Mattsson *et al.* (1): $S_{eff}(q)$ for a suspension of microgels at ϕ_{eff} = 0.12 (□), 0.15 (□), 0.29 (□), 0.75 (□), 0.89 (○), 1.5 (○), 1.83 (○), 2.4 (○), 3.6 (○), 4.2 (○). (*B*) This work: $S_{eff}(q)$ for casein micelle dispersions. The purple and pink curves are the experimental data for C = 150 and 400 g/L, respectively.

The *homogeneous* model describes the casein micelle as a homogeneous network of casein macromolecules that is cross-linked by randomly located CaP nanoclusters (2,3). Under compression, such a network would behave as the microgel particles studied by Mattsson *et al.* (1), which are uniformly compressed and do not interpenetrate. This behavior is characteristic of an affine deformation in which all distances shrink by the same factor.

In order to quantitatively analyse the deformation field, we follow the analysis of Mattsson *et al.* (1), and we define an effective structure factor $S_{eff}(q)$ as the ratio of the scattered intensities in the concentrated and in the dilute dispersion. Fig. S1 *A* shows the variation of $S_{eff}(q)$ for the microgel particles, reproduced from ref. (1). In the dilute dispersions, $S_{eff}(q)$ shows a depression followed by a peak, caused by the correlations of positions of neighboring microgel particles. In concentrated dispersions, $S_{eff}(q)$ is essentially translated along to higher q values, as all distances between and within the microgel particles shrink by the same ratio.

Fig. S1 *B* compares the prediction for the *homogeneous* model with the experimental SAXS curves of the casein micelles. The purple curve is the structure factor at a concentration C = 150 g/L ($\phi_{eff} \approx 0.66$), where the micelles are closely packed but not yet deformed by the compression. The solid black line is the prediction for a compression to C = 400 g/L of this dispersion, according to an affine deformation, as expected for a crosslinked gel particle. The pink curve is the experimental structure factor of casein micelles. The very broad depression observed in the experimental $S_{eff}(q)$ indicates that the deformation of the micellle is not affine. Contrary to the prediction of the *homogeneous* model, there must be dense and less dense regions within the micelle, and the broad depression is caused by the collapse of the less dense regions.

S1-2 *Core-shell* model

"In silico" compression of a core-shell structure: a form-factor analysis

The simple core-shell model presented here is inspired from the recent work of Shukla *et al.* (4). The casein micelle is considered as a polydisperse particle made of a uniform casein matrix that contains CaP nanoclusters. The nanoclusters are located more preferentially at the periphery of the micelle, forming the "shell" of higher electron density than the internal "core". As in the work of Shukla *et al.*, we considered that the scattered intensity is the sum of two contributions:

$$I(q) = I_{cs}(q) + I_{nc}(q) \qquad \text{(S1)}$$

with $I_{cs}(q)$ the intensity scattered by the polydisperse core-shell particles and $I_{nc}(q)$ the intensity scattered by the CaP nanoclusters.

Both contributions were estimated using the SASfit software package (5). For $I_{nc}(q)$, a model of hard spheres with a log-normal distribution was used. For $I_{cs}(q)$, the "Spherical Shell ii" structural model was used (depicted in Fig. S2), assuming a log-normal distribution of global radii as well. Particle interactions were ignored in the calculations so that the calculated scattering intensities correspond to the form factor of the particle.

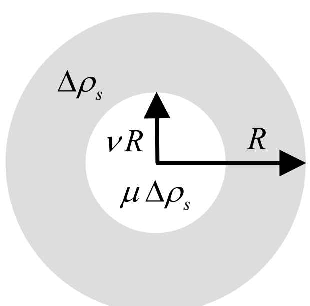

FIGURE S2 The "Spherical Shell ii" SASfit structural model. This structure is characterized through 2 size (R, μ) and 2 contrast (ν, $\Delta\rho_s$) parameters. For clarity, we use the same terminology as in the SASfit software.

The model was first used to fit the data obtained at low concentration (C = 25 g/L). A very good fit was obtained with the parameters listed in Table S1 (Fig. S3 *A*, *B* and *C*).

TABLE S1 Parameters values obtained from the fit of the *core-shell* model to the experimental data at C = 25 g/L. We set the contrast of the CaP nanoclusters at 1 (arbitrary unit, a.u.) and we considered that the CaP nanoclusters number density was 1000 times greater than the casein micelle number density (there are ~1000 CaP nanoclusters in an average micelle (2)).

Core-shell structure		Nanoclusters	
Number density, N_i (a.u.)	3.34×10^{-12}	N_{nc} (a.u.)	3.34×10^{-9}
Average radius, R_i (nm)	34.6	R_{nc} (nm)	1.7
Polydispersity σ_{cs}	0.4	σ_{nc}	0.2
ν_i	0.69	-	-
μ_i	0.45	-	-
$\Delta\rho_{s,i}$ (a.u.)	0.21	$\Delta\rho_{nc}$ (a.u.)	1

Compressions "in silico" were then performed by calculating the intensity scattered by the same object after compression. For that purpose, we estimated the new SASfit input parameters using the following general equations:

$$R_f = \alpha R_i \tag{S2}$$

$$\Delta\rho_{s,f} = \Delta\rho_{s,i} \frac{\left(1-\nu_i^3\right)}{\alpha^3\left(1-\nu_f^{\,3}\right)} \tag{S3}$$

$$\mu_f = \mu_i \frac{\nu_i^3\left(1-\nu_f^{\,3}\right)}{\nu_f^{\,3}\left(1-\nu_i^3\right)} \tag{S4}$$

with i standing for the initial state and f for the state after compression. For C = 400 g/L dispersion, we estimated α to be comprised between 0.7 and 0.85; assuming the micelle actually deforms between 150 g/L ($\phi \approx 0.66$) and 230 g/L ($\phi \approx 1$), respectively.

It was also necessary to consider three possible scenarios regarding the deformation of the core-shell structure, each scenario giving an additional relationship between ν_i and ν_f:

. *Affine deformation* (the shell and the core are equally compressed)

$$\nu_f = \nu_i \tag{S5}$$

. *Deformation of the shell only* (the core is intact)

$$\nu_f = \frac{\nu_i}{\alpha} \tag{S6}$$

. *Deformation of the core only* (the shell thickness is constant)

$$\nu_f = 1 - \frac{1-\nu_i}{\alpha} \tag{S7}$$

TABLE S2 The input parameters values calculated from Eqs. S2 to S7 and used for the SASfit calculations. N_i, σ_{cs}, and the nanoclusters parameters values were taken from Table S1. In the second scenario, the maximum compression is attained at α = 0.78 when the shell thickness equals the diameter of a CaP nanocluster.

	Affine deformation		Shell deformation		Core deformation	
	$\alpha = 0.85$	$\alpha = 0.7$	$\alpha = 0.85$	$\alpha = 0.78$	$\alpha = 0.85$	$\alpha = 0.7$
R_f (nm)	29.4	24.3	29.4	27.1	29.4	24.3
ν_f	0.69	0.69	0.81	0.88	0.63	0.55
μ_f	0.45	0.45	0.19	0.10	0.64	1.06
$\Delta\rho_{s,f}$ (a.u.)	0.34	0.61	0.49	0.90	0.31	0.49

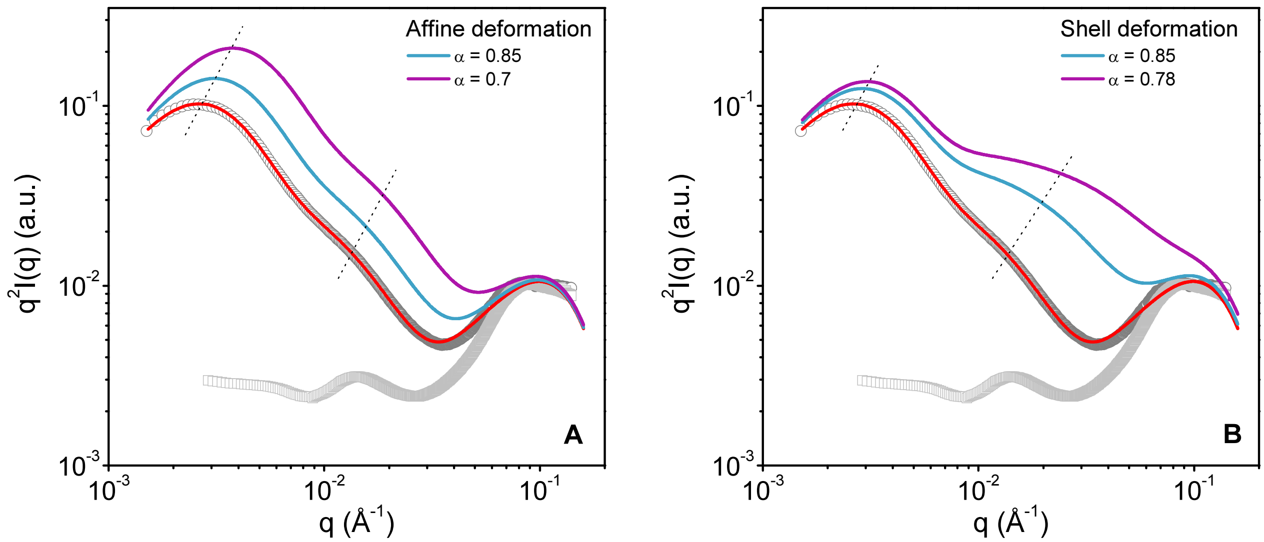

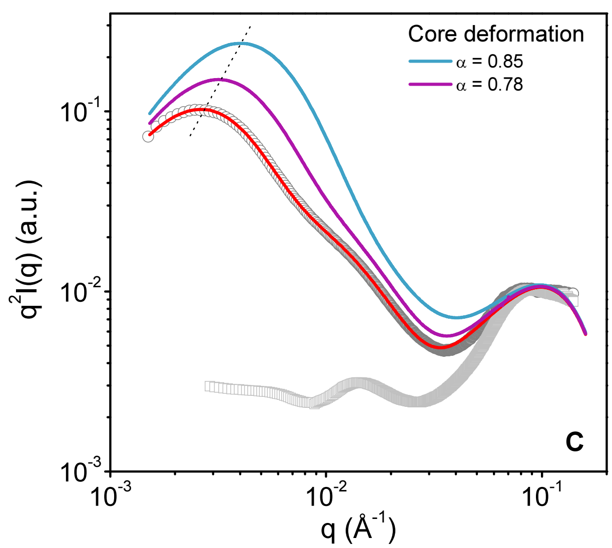

FIGURE S3 The SASfit calculated intensity for a core-shell structure under compression: (*A*) affine deformation, (*B*) deformation of the shell only, (*C*) deformation of the core only. The symbols are the experimental intensities obtained at "native" concentration (25 g/L, *open circles*) and after extreme osmotic compression (400 g/L, *open squares*). The red line is the best fit before compression (Table S1). The blue and purple lines are the intensities calculated at different degrees of compression (Table S2). The dotted lines help in locating the intensity shifts induced by the compression.

The estimated parameters are listed in Table S2 for each scenario. The calculated intensities are presented in Fig. S3 *A*, *B* and *C*. In the two first cases, the compression induces both an increase in magnitude and a shift in the *q*-position of the first and intermediate peaks of the SAXS curve (Fig. S3 *A* and *B*). In the third case, the compression makes the core-shell structure more uniform in density so that the intermediate peak becomes less visible (Fig. S3 *C*).

Clearly, none of these variations matches those obtained experimentally (= loss of relative intensity of the two first peaks and constant *q*-position of the intermediate peak). Moreover, it is unlikely that particle interactions, which are ignored in our calculations, are responsible for this mismatch, even if such interactions are potentially strong in a context of concentrated dispersions of core-shell particles. Accordingly, it seems quite difficult to conciliate the *core-shell* model recently proposed by Shukla *et al.* (4) and the SAXS data we obtained from compressed casein micelle dispersions.

S1-3 Presence of *mini-micelles*

Calculated SAXS intensities with two coexisting populations of casein micelles

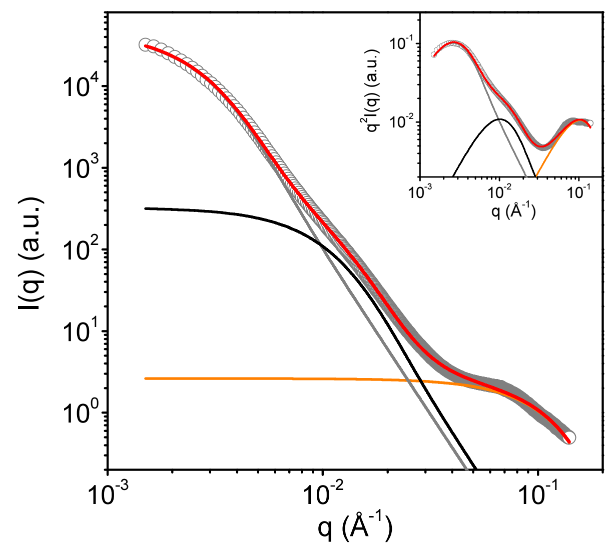

FIGURE S4 The SAXS intensities of a 25 g/L casein micelle dispersion (open circles) together with the best fit of the form-factor model of Gebhardt *et al.* (red line) (6–8). The contributions of each structural element *n* to the global fit are displayed as well: casein micelles (n = 0, gray line), hypothetical *mini-micelles* (n = 1, black line) and CaP nanoclusters (n = 2, orange line).

Fig. S4 shows the SAXS data we obtained from a dispersion at "native" concentration, i.e., at 25 g/L. The red line represents the intensities calculated from a form-factor model that is identical to the one used by Gebhardt *et al.* in GISAXS studies of dry thin films of casein micelles (6–8). In this model, intensity $I(q)$ is the sum of the intensities scattered by the casein micelles (level 0) together with a separate population of small micelles called *mini-micelles* (level 1) and the CaP nanoclusters (level 2). The effects of interactions between the objects are not taken into account so that the intensity is given by:

$$I(q) = c\left[\phi_0 v_0 (\Delta\rho_0)^2 P_0(q) + \phi_1 v_1 (\Delta\rho_1)^2 P_1(q) + \phi_2 v_2 (\Delta\rho_2)^2 P_2(q)\right] \quad \text{(S8)}$$

where c is a constant accounting for the total concentration in caseins. ϕ_{n} is the volume fraction occupied by the structural element n in the dispersion, while v_n and $\Delta\rho_n$ are its volume and average scattering contrast, respectively. $P_n(q)$ are the form factors of each object.

In our calculations, we assumed that $P_n(q)$ are the form factors of polydisperse hard spheres that follow a Schulz size distribution with a number average diameter d_n and polydispersity σ_n. We used the expressions of Aragon *et al.* to estimate those form factors (9). The d_n and σ_n values we obtained from an adequate fit to our data at 25 g/L are given in Table S3. The average size we obtained for the putative *mini-micelles* population is quite similar (despite a little bit higher) to the one calculated by Gebhardt *et al.* with thin films of casein micelles (6–8).

TABLE S3 Parameters obtained from the best fit of the "form factor model" to the casein micelle SAXS profile at C = 25 g/L.

Structural level	d_n (nm)	σ_n
n = 0, casein micelles	73.1	0.50
n = 1, hypothetical *mini-micelles*	20.9	0.45
n = 2, CaP nanoclusters	3.4	0.20

Such a fit of Eq. S8 to our data makes possible to estimate the relative importance of the hypothetical *mini-micelles* population compared to the population of "regular" casein micelles. To reproduce the hump observed at intermediate q values, it is indeed necessary to set a ratio $\frac{\phi_0 v_0 \left(\Delta\rho_0\right)^2}{\phi_1 v_1 \left(\Delta\rho_1\right)^2} \approx 150$. Knowing the average dimensions of the casein micelles and the *mini-micelles* (Table S3) and assuming that the scattering contrast of the *mini-micelles* is equal or inferior to the micelles contrast ($\Delta\rho_0 \geq \Delta\rho_1$), we found $\phi_1/\phi_0 \geq 0.28$. Converted into a number ratio, this suggests that *mini-micelles* would be 12 times more numerous than "regular" casein micelles. However, the latest electron microscopy images obtained with casein micelle dispersions (either made from "fresh" skimmed milk or NPC powder) do not show any evidence of such a large population of *mini-micelles* (10–12).

Dynamic light scattering

To gain further information about the hypothetical presence of *mini-micelles* in our dispersions, we performed a series of dynamic light scattering (DLS) experiments. The *mini-micelles* hypothesis indeed originates from DLS measurements made by Muller-Buschbaum *et al.* with dispersions at $C \leq 30$ g/L (13). The DLS data we obtained in the same experimental conditions and with a very similar apparatus are given in Fig. S5, *A* and *B*. Clearly, DLS was not able to detect any objects with diameters < 50 nm in our case and a single population of "regular" casein micelles was sufficient to accurately describe the measured intensity correlation function.

Additionally, we performed measurements with DLS instruments of various optical configurations (Fig. S6). In particular, we used an instrument that combines DLS in the backscattering mode with thin layer measurements and that is, in theory, more able to measure "difficult" size distributions (VASCO Particle Size Analyzer, Cordouan Technologies, Pessac, FR). Again, none of these results indicated the presence of small objects with diameters < 50 nm.

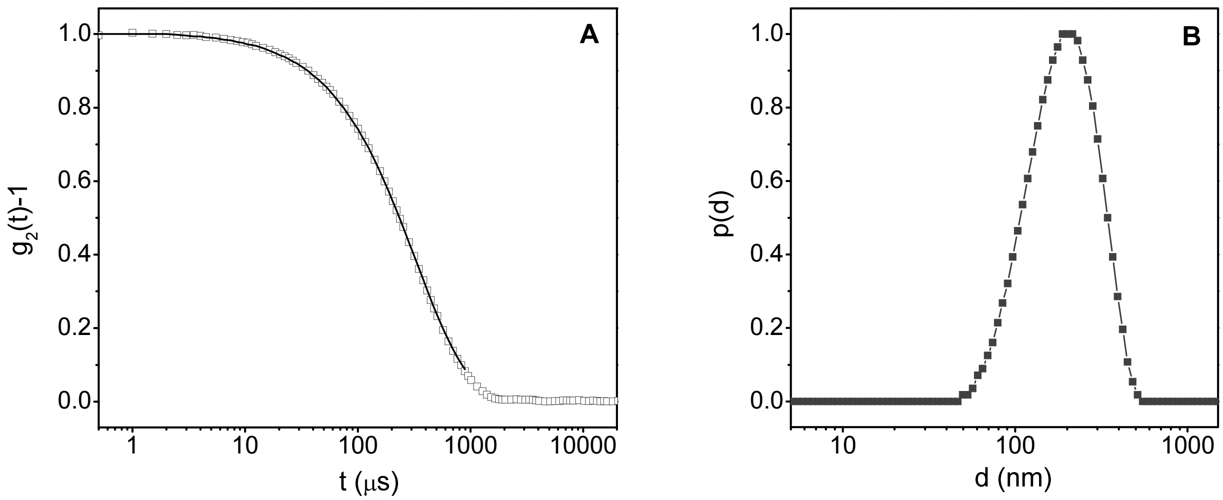

FIGURE S5 (*A*) DLS intensity correlation function $g_2(t)-1$ of a casein micelle dispersion made from NPC+UF at 2.5 g/L casein concentration (*open squares*). The solid line shows the fit calculated with the size distribution of Fig. S5 *B*. The measurement was performed in backscattering mode at angle 173° and temperature 20°C with a Zetasizer Nano ZS instrument (Malvern Instruments, Malvern, UK). (*B*) The calculated intensity size distribution function *p*(*d*) as a function of casein micelle diameter *d*.

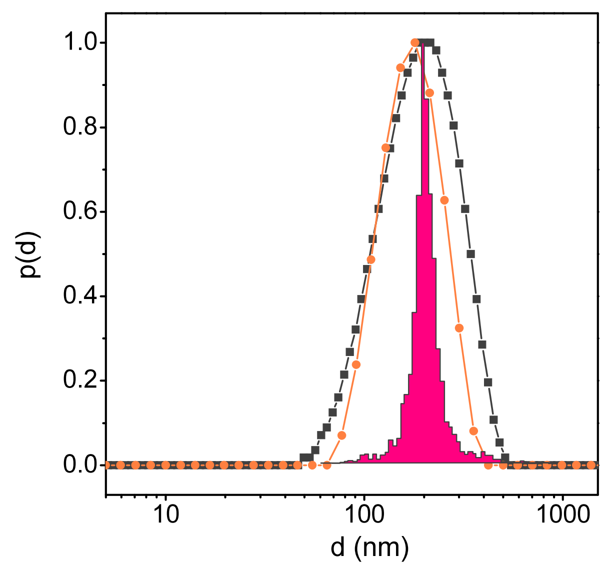

FIGURE S6 The intensity size distribution function *p*(*d*) of casein micelle dispersions made from NPC+UF: casein concentration *C* = 0.25 g/L, Zetasizer 3000 HS (Malvern Instruments, Malvern, UK), angle 90°, CONTIN algorithm (*black squares*); *C* = 2.5 g/L, Zetasizer Nano ZS instrument (Malvern Instruments, Malvern, UK), backscattering mode at angle 173°, CONTIN algorithm (*orange circles*); *C* = 25 g/L, thin layer measurement, VASCO Particle Size Analyzer (Cordouan Technologies, Pessac, FR), backscattering mode at angle 135°, multi-acquisition and Padé-Laplace algorithm (*pink-filled area*). All measurements were performed at 20°C.

As it was still possible that the presence of the "regular" casein micelles makes the signal of *mini-micelles* hardly detectable, we performed other DLS experiments with dispersions in which casein micelles were partially removed by ultracentrifugation (Fig. S7). Ultracentrifugation was done at 70 000 × g and 20°C with a Sorvall Discovery 90 SE ultracentrifuge (Hitachi, USA) and the casein concentration in the supernatants was determined using the Bradford method (14). The total amount of casein removed was ~78 % after 30 min centrifugation. According to our previous estimation of the volume fraction occupied ϕ_1 by the hypothetical *mini-micelles* ($\phi_1/\phi_0 \geq 0.28$), such a percentage is theoretically sufficient to make the *mini-micelles* population visible in DLS. Fig. S7 shows that this partial elimination of casein led to a global shift of the micelles intensity size distribution towards lower sizes, which was expected. On the other hand, DLS was not able to detect a distinct population of objects at the sizes expected for the *mini-micelles*, i.e. between 10 and 50 nm.

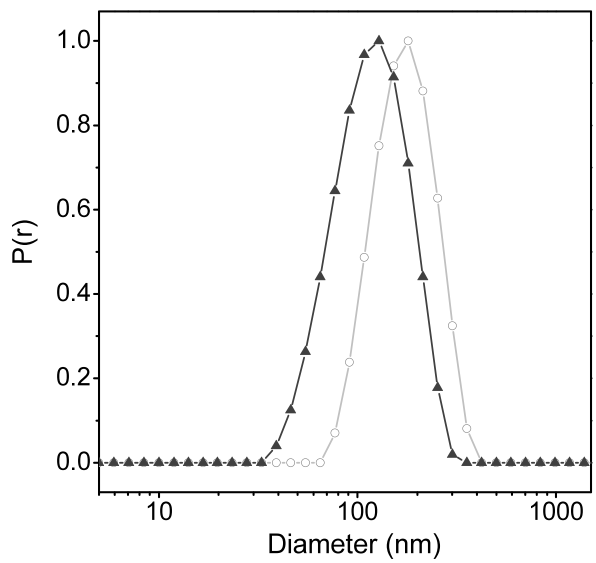

FIGURE S7 The intensity size distribution function $p(d)$ of a casein micelle dispersion made from NPC+UF at C = 0.25 g/L (*empty circles*) and of supernatants obtained after 30 min ultracentrifugation at 70 000 g of a 25 g/L dispersion made from NPC+UF (*black triangles and green diamonds*). After ultracentrifugation, ~78 % of the caseins were removed. All measurements were performed at 20°C.

As a conclusion of this note, we think it is quite reasonable to assume that *mini-micelles* are not present in our dispersions, or, at least, are not enough numerous to contribute to the SAXS profiles we present in the article.

Note S2: Sponge model

Quality of the fits and parameters obtained

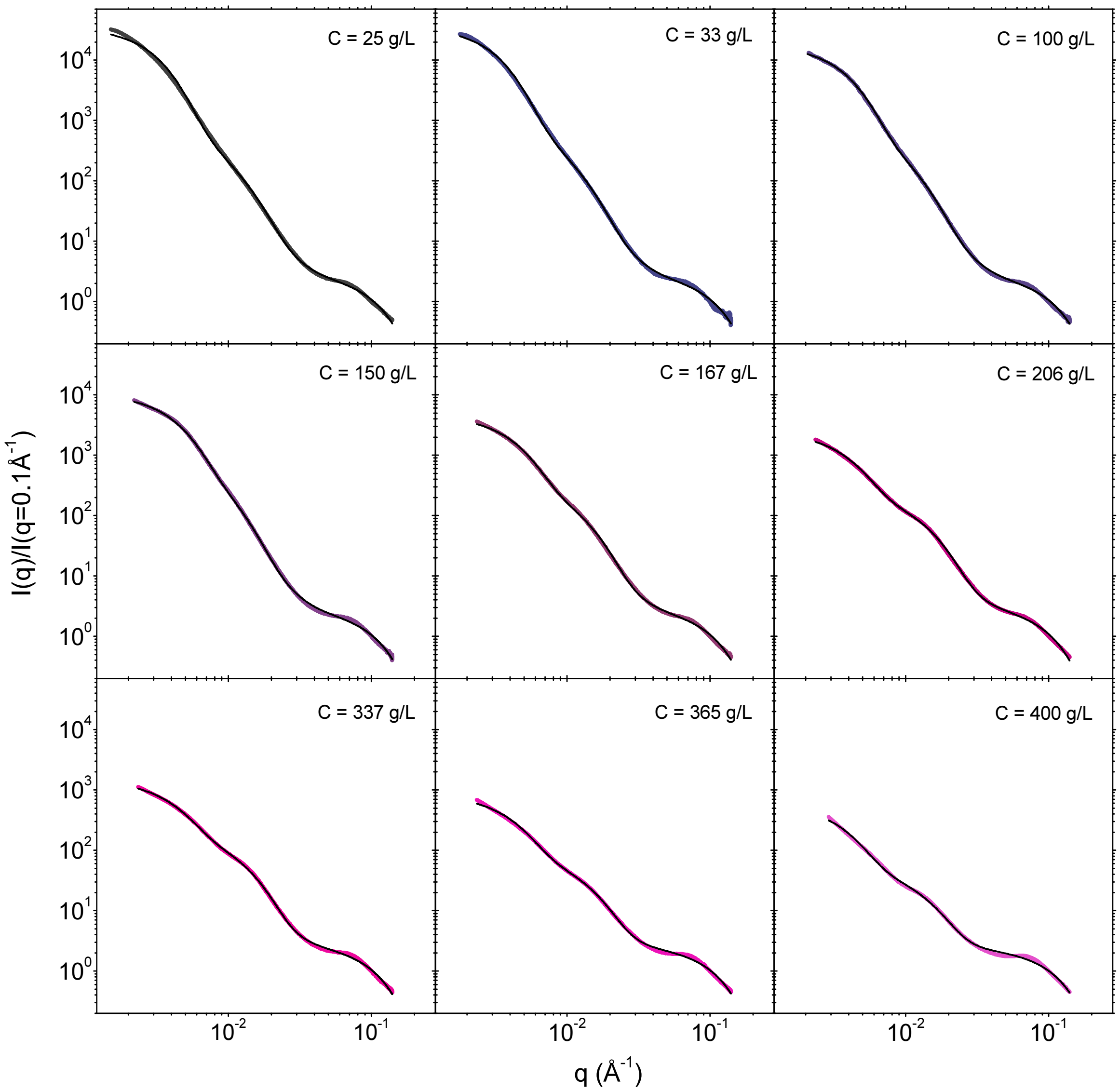

FIGURE S8 Modeling of the SAXS intensities of compressed casein micelle dispersions. The thick colored lines are the experimental data. The thin black lines show the best fits to the model.

In our article, we propose to describe our SAXS data with a cell model having 3 distinct levels of structure: the micelle (level 0), some "hard" regions within the micelle (level 1), and the CaP nanoclusters (level 3) (see text and Eqs. 2 to 5). Fig. S8 above is an alternative view of the fits of the data to this model. The agreement is excellent in all cases.

In the calculations of $I(q)$ with Eq. 2, we assumed that $P_n(q)$ are the form factors of polydisperse hard spheres that follow a Schulz size distribution with a number average diameter d_n and polydispersity σ_n and we used the expressions of Aragon *et al.* to estimate those form factors (9). Additionally, in order to minimize the number of free parameters in the model, we set the σ_n values to realistic ones, i.e. $\sigma_n = 1/3$ for the micelles ($n = 0$) and the "hard" regions ($n = 1$) and $\sigma_2 = 0.2$ (CaP nanoclusters). So only the pre-factors a, b and c, and the diameters d_n were varied to fit the data at each concentration. The parameters obtained from the fits are listed in Table S4. Fig. S9 gives the size distributions that correspond to the three structural levels of the model for $C = 25$ g/L.

TABLE S4 Parameters obtained from the fits of the model to the experimental data.

	Level 0 - Micelle			Level 1 - "Hard" regions			level 2 - CaP nanoclusters		
C (g/L)	a	d_0 (nm)	σ_0	b	d_1 (nm)	σ_1	c	d_2 (nm)	σ_2
25	34678.8	92.0	0.33	251.3	24.6	0.33	2.6	3.4	0.20
33	35405.0	89.0	0.33	322.6	25.6	0.33	2.7	3.4	0.20
100	17499.4	76.1	0.33	299.6	25.9	0.33	2.6	3.4	0.20
150	9998.6	67.0	0.33	396.8	28.6	0.33	2.6	3.4	0.20
167	4323.5	66.1	0.33	219.2	21.9	0.33	2.7	3.5	0.20
206	2258.5	72.4	0.33	172.2	20.1	0.33	3.0	3.6	0.20
337	1317.1	68.8	0.33	148.9	21.9	0.33	2.6	3.4	0.20
365	765.1	68.8	0.33	64.9	20.3	0.33	2.5	3.3	0.20
400	558.3	77.0	0.33	39.8	20.8	0.33	2.3	3.2	0.20

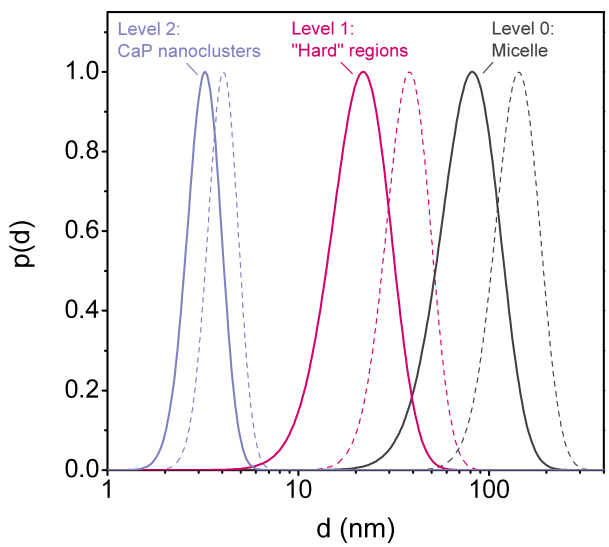

FIGURE S9 The size distribution functions $p(d)$ obtained from the best fits of our model to the SAXS data at $C = 25$ g/L. In our calculations, we implicitly assumed that the pseudo-form factors $P_0(q)$, $P_1(q)$ and $P_2(q)$ in Eq. 2 are form factors for polydisperse hard spheres. The solid lines are the number size distributions that were directly used for the calculation of the pseudo-form factors through the expressions of Aragon et al. (9). The dashed lines are the corresponding "intensity" size distributions assuming $I \propto d^6$. For the casein micelle (level 0), this distribution matches that measured through dynamic light scattering (see Fig. S5 *B* or ref (15)).

Calculation of ϕ_0, ϕ_1 and ϕ_2 as a function of casein concentration

Knowing, the values of the prefactors *a*, *b* and *c*, it is possible to estimate the volume fractions ϕ_0, ϕ_1 and ϕ_2 that appear in the model. For that purpose, we use the following expressions, deduced from Eqs. 3-5:

$$\phi_1 = 1 - \left[\frac{b}{c} \frac{(\Delta\rho_2)^2}{(\Delta\rho_1)^2} \left(\frac{d_2}{d_1} \right)^3 \phi_2 (1 - \phi_2) \right] \quad \text{(S9)}$$

$$\phi_0 = 1 - \left[\frac{a}{b} \frac{(\Delta\rho_1)^2}{(\Delta\rho_0)^2} \left(\frac{d_1}{d_0} \right)^3 \phi_1 (1 - \phi_1) \right] \quad \text{(S10)}$$

For simplicity, we also make the following hypothesis:

. The "hard" regions are not compressed in the concentration range investigated, which seems very reasonable since the characteristic dimension D_1^* does not change during compression. This implies that ρ_1, $\Delta\rho_2$, and ϕ_2 do not change with concentration.

. The average scattering of the micelle, $\Delta\rho_0$, does not change with concentration. This hypothesis is questionable since we know the micelle is compressed and looses solvent at high compression. However, we have no rationale to estimate the increase in $\Delta\rho_0$ that would result from the compression (When does the compression start? What is the balance between deformation and deswelling? ;..). Moreover, we found that such an increase, even if exaggerated, does not induce any significant changes in the general variation of ϕ_n with *C* (results not shown).

. The "hard" regions contain all the CaP and protein materials and are separated by voids filled with solvent. This gives the following relation between $\Delta\rho_0$ and $\Delta\rho_1$ for the uncompressed micelle:

$$\Delta\rho_1 = \Delta\rho_0 \left(\frac{1 - \phi_1}{\phi_1} \right) \quad \text{(S11)}$$

. The CaP nanoclusters occupy ~1% of the micelle volume (2), leading to this other simple relation for the uncompressed micelle :

$$(\phi_1 \phi_2) \approx 0.01 \quad \text{(S12)}$$

Table S5 gives the electron densities we estimate for the solvent (ρ_{UF}), the overall micelle (ρ_0) and the CaP nanoclusters (ρ_2), using relevant references. The calculation then first consists in setting ϕ_2 at an initial value close to 0.01 and estimating the contrast parameters $\Delta\rho_1$ from Eqs. S12 and S11, and $\Delta\rho_2$ from $\Delta\rho_2 = \rho_2 - \rho_1$. Knowing all the contrast parameters, Eqs. S9 and S10 were then used to calculate ϕ_0 and ϕ_1 for all concentrations using the data of Table S5. If the volume fractions ϕ_1 calculated for the lowest concentrations were too different from $0.01/\phi_2$ (Eq. S12), ϕ_2 was increased by a small increment and the calculation repeated. This procedure was continued until the condition (S12) was satisfied at low concentration, i.e., when the micelle is not compressed. A final value of 0.02 was found for ϕ_2. The corresponding contrast parameters are given in Table S5 and the resulting values of ϕ_0 and ϕ_1 are given in Fig. 5 *A* of the article.

Fig. S10 gives the electron density of each structural level relative to the electron density of the solvent.

TABLE S5 Parameters used for the calculation of ϕ_0 and ϕ_1 from the fits of the hierarchical model to the SAXS patterns of compressed casein micelle dispersions.

Parameter	Value	Calculation method and/or reference(s)
ρ_{UF} (solvent electron density)	350 e^-/nm^3	. water electron density ρ_w = 334 e^-/nm^3 . ion composition of ref. (16) . lactose concentration ~46 g/L
ρ_2 (nanoclusters electron density)	539 e^-/nm^3	. an average nanocluster of diameter 4.8 nm contains 355 $CaHPO_4 \cdot 2H_2O$ units, ref. (17)
ρ_0 (micelle electron density)	365 e^-/nm^3	. micelle voluminosity = 4.4 mL/g, ref. (15) . casein e^- density = 3.16 x 10^{23} e^-/g, ref. (18) . casein specific volume = 0.736 mL/g, ref. (18) . 7 g of CaP per 100 g of dry casein, refs. (2,19)
ρ_1 (electron density of the "hard" regions within the micelle)	381 e^-/nm^3	. Eqs. S11 and S12
$\Delta\rho_0 = \rho_0 - \rho_{UF}$	15 e^-/nm^3	-
$\Delta\rho_1 = \rho_1 - \rho_0$	16 e^-/nm^3	-
$\Delta\rho_2 = \rho_2 - \rho_1$	158 e^-/nm^3	-
ϕ_2	0.02	-

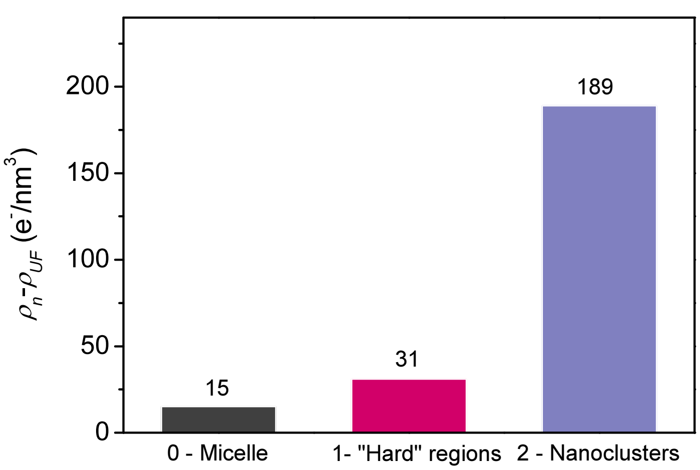

FIGURE S10 The estimated electron density of the three structural levels n = 0 (micelle), 1 (the "hard" regions) and 2 (CaP nanoclusters), relative to the electron density of the solvent (ρ_{UF} = 350 e^-/nm^3).

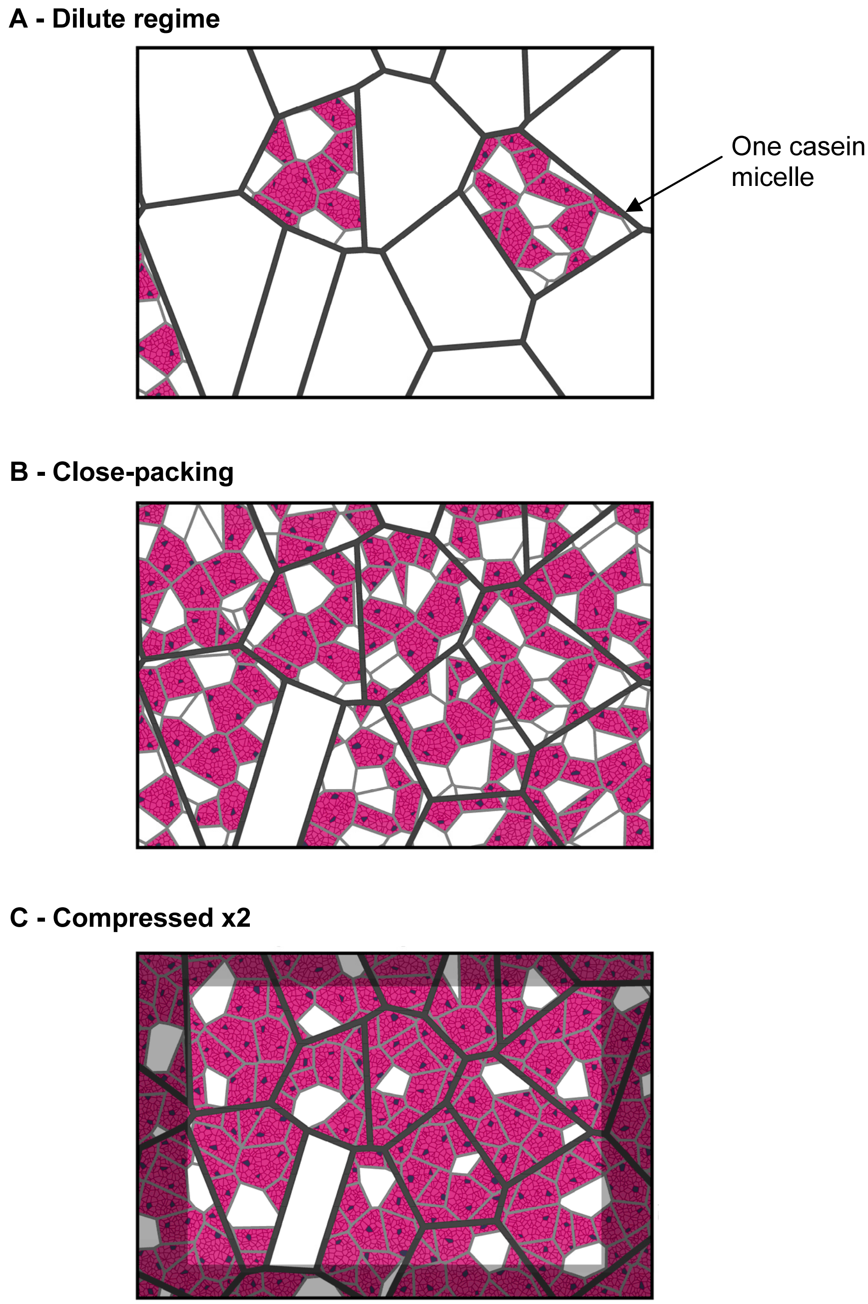

FIGURE S11 The different consecutive states of the casein micelle during compression according to the *sponge model* (highly schematic). Following our description of the model, the dispersion is decomposed into Voronoi cells that either contain casein micelles (see Fig. 6 of the article) or solvent (blank cells) *(A)* Dilute regime: the micelles are still separated from each other. Half of their internal structure is made of voids filled with solvent ($\phi_1 \approx 0.5$) *(B)* Close-packing: in their great majority, the micelles are in direct contact ($\phi_0 \approx 1$) but their internal structure is not yet affected ($\phi_1 \approx 0.5$). *(C)* Compressed x2: the micelles are compressed such that their volume is twice lower than in the initial state. The "hard" regions have been pushed closer together so that the majority of the voids that composed the internal structure have collapsed ($\phi_1 \approx 0.5$).

References

1. Mattsson, J., H. M. Wyss, A. Fernandez-Nieves, K. Miyazaki, Z. Hu, D. R. Reichman, and D. A. Weitz. 2009. Soft colloids make strong glasses. *Nature*. 462:83-86.

2. Holt, C., C. G. De Kruif, R. Tuinier, and P. A. Timmins. 2003. Substructure of bovine casein micelles by small-angle X-ray and neutron scattering. *Colloids Surf. , A*. 213:275-284.

3. Marchin, S., J. L. Putaux, F. Pignon, and J. Léonil. 2007. Effects of the environmental factors on the casein micelle structure studied by cryo transmission electron microscopy and small-angle X-ray scattering/ultrasmall-angle X-ray scattering. *J. Chem. Phys.* 126:045101-045110.

4. Shukla, A., T. Narayanan, and D. Zanchi. 2009. Structure of casein micelles and their complexation with tannins. *Soft Matter*. 5:2884-2888.

5. Kohlbrecher, J. and I. Bressler. SASfit version 0.92.3. http://kur.web.psi.ch/sans1/SANSSoft/sasfit.html. Accessed June 9, 2010.

6. Gebhardt, R., M. Burghammer, C. Riekel, S. Volkher Roth, and P. Müller-Buschbaum. 2008. Structural changes of casein micelles in a calcium gradient film. *Macromol. Biosci.* 8:347-354.

7. Gebhardt, R., M. Burghammer, C. Riekel, U. Kulozik, and P. Müller-Buschbaum. 2010. Investigation of surface modification of casein films by rennin enzyme action using micro-beam grazing incidence small angle X-ray scattering. *Dairy Sci. Technol.* 90:75-86.

8. Gebhardt, R., S. V. Roth, M. Burghammer, C. Riekel, A. Tolkach, U. Kulozik, and P. Müller-Buschbaum. 2010. Structural changes of casein micelles in a rennin gradient film with simultaneous consideration of the film morphology. *Int. Dairy J.* 20:203-211.

9. Aragon, S. R. and R. Pecora. 1976. Theory of dynamic light scattering from polydisperse systems. *J. Chem. Phys.* 64:2395-2404.

10. McMahon, D. J., H. Du, W. R. McManus, and K. M. Larsen. 2009. Microstructural changes in casein supramolecules during acidification of skim milk. *J. Dairy Sci.* 92:5854-5867.

11. Knudsen, J. C. and L. H. Skibsted. 2010. High pressure effects on the structure of casein micelles in milk as studied by cryo-transmission electron microscopy. *Food Chemistry*. 119:202-208.

12. Martin, A. H., H. D. Goff, A. Smith, and D. G. Dalgleish. 2006. Immobilization of casein micelles for probing their structure and interactions with polysaccharides using scanning electron microscopy (SEM). *Food Hydrocolloids*. 20:817-824.

13. Müller-Buschbaum, P., R. Gebhardt, S. V. Roth, E. Metwalli, and W. Doster. 2007. Effect of calcium concentration on the structure of casein micelles in thin films. *Biophys. J.* 93:960-968.

14. Bradford, M. M. 1976. A rapid and sensitive method for the quantitation of microgram quantities of protein utilizing the principle of protein-dye bonding. *Anal. Biochem.* 72:248-254.

15. De Kruif, C. G. 1998. Supra-aggregates of casein micelles as a prelude to coagulation. *J. Dairy Sci.* 81:3019-3028.

16. Jenness, R. and J. Koops. 1962. Preparation and properties of a salt solution which simulates milk ultrafiltrate. *Neth. Milk Dairy J.* 16:153-164.

17. Holt, C., P. A. Timmins, N. Errington, and J. Leaver. 1998. A core-shell model of calcium phosphate nanoclusters stabilized by beta-casein phosphopeptides, derived from sedimentation equilibrium and small-angle X-ray and neutron-scattering measurements. *Eur. J. Biochem.* 252:73-78.

18. Farrell, H. M., Jr., H. Pessen, E. M. Brown, and T. F. Kumosinski. 1990. Structural insights into the bovine casein micelle: small angle X-ray scattering studies and correlations with spectroscopy. *J. Dairy Sci.* 73:3592-3601.

19. Walstra, P., A. T. J. M. Woutersen, and T. J. Geurts. 2006. Dairy Science and Technology. CRC Taylor & Francis, Boca Raton, FL.